

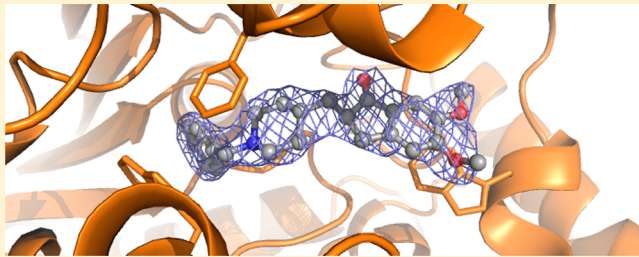
Conformational Analysis and Parallel QM/MM X-ray Refinement of Protein Bound Anti-Alzheimer Drug Donepezil

Zheng Fu, Xue Li, Yipu Miao, and Kenneth M. Merz, Jr.*

Department of Chemistry and the Quantum Theory Project, 2328 New Physics Building, P.O. Box 118435, University of Florida, Gainesville, Florida 32611-8435, United States

Supporting Information

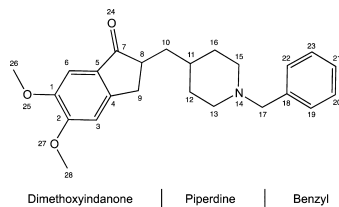
ABSTRACT: The recognition and association of donepezil with acetylcholinesterase (AChE) has been extensively studied in the past several decades because of the former's use as a palliative treatment for mild Alzheimer disease. Herein, we examine the conformational properties of donepezil and we re-examine the donepezil-AChE crystal structure using combined quantum mechanical/molecular mechanical (QM/MM) X-ray refinement tools. Donepezil's conformational energy surface was explored using the M06 suite of density functionals and with the MP2/complete basis set (CBS) method using the aug-cc-pVXZ ($X = D$ and T) basis sets. The donepezil-AChE complex (PDB 1EVE) was also rerefined through a parallel QM/MM X-ray refinement approach based on an in-house ab initio code QUICK, which uses the message passing interface (MPI) in a distributed SCF algorithm to accelerate the calculation via parallelization. In the QM/MM rerefined donepezil structure, coordinate errors that previously existed in the PDB deposited geometry were improved leading to an improvement of the modeling of the interaction between donepezil and the aromatic side chains located in the AChE active site gorge. As a result of the rerefinement there was a 93% reduction in the donepezil conformational strain energy versus the original PDB structure. The results of the present effort offer further detailed structural and biochemical inhibitor-AChE information for the continued development of more effective and palliative treatments of Alzheimer disease.



INTRODUCTION

Donepezil (trade name Aricept), [(R,S)-1-benzyl-4-[(5,6-dimethoxy-1-indanon)-2-yl]methyl)piperidine (see Scheme 1),

Scheme 1. Structure Diagram of Donepezil with Atoms Numbering



is a palliative anti-Alzheimer drug designed based on the assumption that pharmacologically maintaining acetylcholine levels in the brain may alleviate symptoms of Alzheimer's disease (AD).^{1–3} It inhibits the acetylcholinesterase (AChE) enzyme from rapidly hydrolyzing the neurotransmitter acetylcholine at cholinergic synapses of neuronal contacts in the central nervous system, thereby increasing the concentration of acetylcholine in numerous brain regions of AD patients with a long duration of action.⁴ Meanwhile, it has been demonstrated that donepezil neither adversely affects the synthesis of acetylcholine nor inhibits the activity of choline acetyltransferase.^{5,6} Hence, clinical trials have shown a

significant correlation between receiving oral donepezil and the improvement in cognitive and global assessments in patients with Alzheimer's disease particularly in the later stages.^{7–16}

Early ligand-based research on indanone-benzylpiperidines applied quantitative structure–activity relationship (QSAR) methods to a series of indanone-benzylpiperidines synthesized by Eisai^{17,18} because at that time little was known about the structure of acetylcholinesterase (AChE). Due to Sussman and co-workers' efforts, the crystal structure of *Torpedo californica* AChE (TcAChE)¹⁹ and subsequently the donepezil-TcAChE complex^{20,21} were reported. This allowed for the elucidation of the interaction between donepezil and AChE and facilitated posthoc rationalizations of the donepezil binding mode as well. Structurally the TcAChE active site gorge is composed of two ligand-binding sites: the acylation site located at the bottom of the gorge and the “peripheral” anionic binding site in the vicinity of the mouth of the gorge. These two compartments were connected via a narrow bottleneck region predominantly formed by the Phe330 and Tyr121 residues. Compared to acetylcholine, donepezil has an enhanced binding affinity with acetylcholinesterase because its longer scaffold affords the ability to span the two anionic binding sites. In addition

Received: November 4, 2012

Published: February 18, 2013



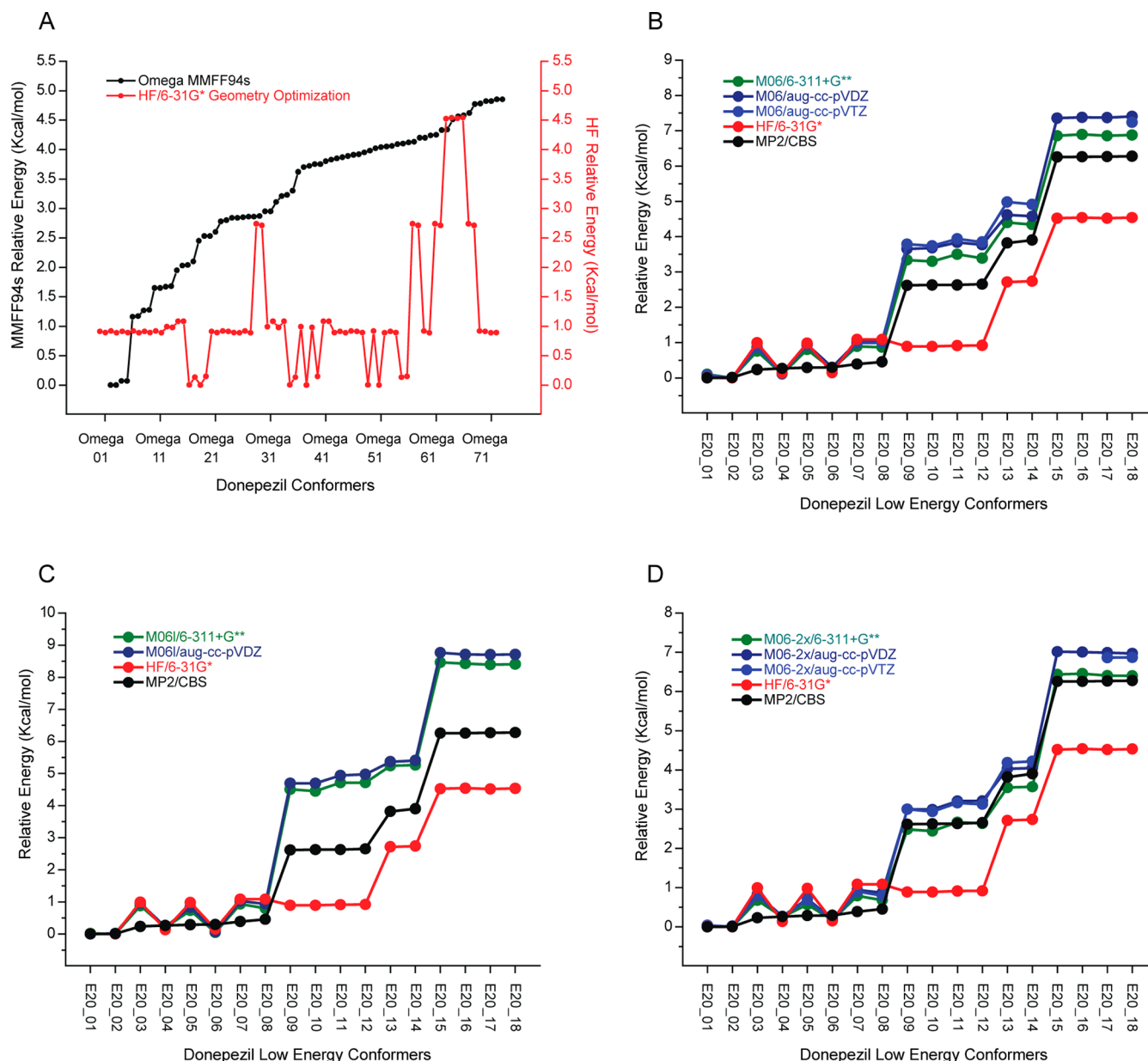


Figure 1. (A) Omega generated donepezil conformational ensembles optimized by HF/6-31G* in gas phase; the relative energies of Omega/ab initio QM methods identified donepezil low-energy conformers were estimated by (B) M06, (C) M062x, and (D) M06l functionals with different basis sets in vacuo and comparing with MP2/CBS results. The 18 donepezil low-energy conformers (*x*-axis) were named in order of increasing MP2/CBS energy.

previous studies articulated there were three major forces stabilizing the donepezil-TcAChE association: (i) a $\pi-\pi$ stacking interaction between the donepezil phenyl group and Trp84 (“sandwich” configuration) at the acylation site; (ii) a $\pi-\pi$ stacking interaction between the indole ring of donepezil and Trp279 (“parallel-displaced” configuration) at the “peripheral” anionic binding site; (iii) a cation– π interaction between the positively charged quaternary ammonium ion of donepezil and Phe330 at the bottleneck region,^{20,21} which results in strong structural complementarity between donepezil and TcAChE. On the basis of the binding pattern of donepezil toward its target enzyme, many groups have undertaken the rational design of donepezil-like compounds via docking and molecular dynamics simulations.^{22–27} Nevertheless, as far as we are aware, none of these workers performed a thorough conformational analysis of donepezil especially in its bound

state. Hence, we describe below the detailed analyses of the conformational preferences of donepezil in both the free and bound state with highly accurate MP2/complete basis set (CBS) methods. Moreover, we employ a parallel QM/MM X-ray refinement methodology^{28–32} to the donepezil-TcAChE complex, thereby providing deeper insights into the AChE inhibitor binding mechanism.

RESULTS

Exploring the Donepezil Conformational Energy Surface. We initially analyzed the donepezil conformational energy surface using Omega,³³ which yielded 66 donepezil conformations all within 5 kcal/mol. All of these Omega generated geometries were fully relaxed at the HF/6-31G* level of theory, which is consistent with the Hamiltonian used in our

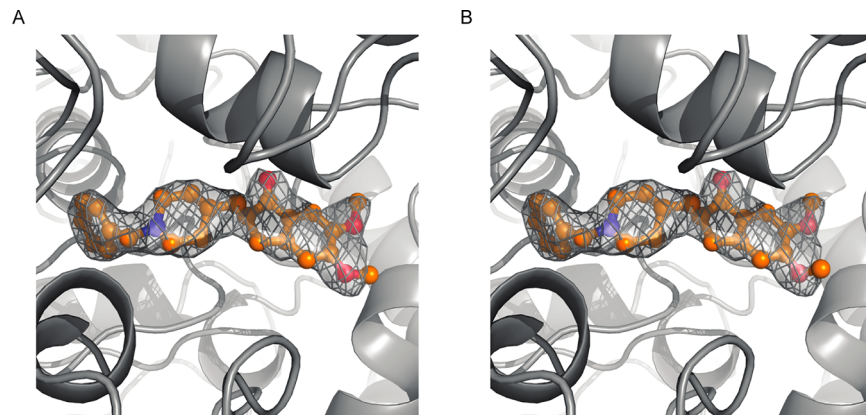


Figure 2. (A) Crystal structure of donepezil in its binding pocket (PDB ID: 1EVE). Electron density ($2F_0 - F_c$) is shown as a wire mesh and reinterpreted at $\sigma = 1.5$ level. (B) Modified donepezil bound conformation.

choice of basis set in the QM/MM X-ray refinement approach. This analysis resulted in 18 unique low-energy donepezil conformations from the original 66 (Figure 1A and Supporting Information Figure 1). In order to gain further insight into the donepezil conformational energy surface, we carried out a series of M06, M06l, and M06-2x single point energy calculations on the predicted local and global energy minima of donepezil, since previous studies afforded us confidence in the performance of M06 class of density functionals on estimating conformational energies of drug-like molecules.^{34–37} Figure 1B shows the relative energy values calculated for the 18 donepezil low-energy conformations using the M06 functional with different basis sets. For E20_01, E20_02, E20_04, and E20_06 the M06 functional computed energies resemble the MP2/CBS results, yet no matter which basis set was selected, they overestimated the MP2/CBS results by about 1–1.5 kcal/mol on the remaining 14 low-energy conformations. The same trend was observed in the M06l curves, and their results were in marked contrast to the MP2/CBS values for the donepezil conformations with higher energies (from E20_09 to E20_18 in Figure 1C, the M06l/aug-cc-pVTZ calculation data was not shown because of SCF convergence issues). For single point calculations with the M06-2x functional (Figure 1D), the DFT computed donepezil conformational energies agree quite well with the MP2/CBS result using either Pople basis set (6-311+G**) or Dunning basis sets (aug-cc-pVDZ and aug-cc-pVTZ). Note that the HF/6-31G* estimated energies are similar to the DFT results on the low-energy donepezil conformations (from E20_01 to E20_08 in Figure 1B, C, and D), yet they were about 2 kcal/mol less than the MP2/CBS values for the remaining higher energy conformers (from E20_09 to E20_18).

Based on the discussion above, one question naturally presents itself: “Is there a quantitative way to tell the difference between DFT and MP2/CBS methods in terms of donepezil conformational energies?” The answer is certainly yes. If we treat the 18 donepezil low-energy conformers as independent “blocks” and different level of theories as “treatments”, we can carry out distribution-free two-side all-treatments multiple comparisons to test our conclusion (Wilcoxon–Nemenyi–McDonald–Thompson Test based on Friedman rank sums). All of the nonparametric statistical inference results are summarized and listed in the Supporting Information. For the 6-311+G** basis set, we have very strong evidence (test statistic = 2, which is much less than the critical value = 18.66 at

$\alpha = 0.05$ level) indicating that the M06-2x and MP2/CBS outcomes are well matched and weak evidence (test statistic = 16, which is close to the critical value = 18.66 at the $\alpha = 0.05$ level) to declare that there is no significant difference between M06 and MP2/CBS results, while we reject the null hypothesis (p -value < 0.05) that the M06l/6-311+G** and MP2/CBS methods are equivalent with respect to the donepezil conformational energies. For the aug-cc-pVDZ and aug-cc-pVTZ, we have reached the conclusion that only M06-2x functional is not different from the MP2/CBS method (fails to reject the null hypothesis with p -value > 0.05), whereas neither M06 nor M06l, with these basis sets, yield results comparable to the MP2/CBS outcome. So in summary, in comparison with the M06l and M06 functionals, only the M06-2x level of theory provides reliable estimates of how much the conformational energy changes among different donepezil fully relaxed geometries. Hence, our suggestion would be to use this level of theory to gain insight into the conformational preferences of small molecules that have similar structures to donepezil (potential drug candidates for the treatment of Alzheimer’s disease) at a reduced computational cost relative to MP2/CBS methods.

Parallel QM/MM Refinement of Donepezil-TcAChE Complex Crystal Structure. Even though donepezil is a very important drug molecule in treating Alzheimer disease, only one donepezil-acetylcholinesterase complex crystal structure has been deposited in the PDB database with a resolution of 2.50 Å (PDB entry 1EVE, *Torpedo californica* acetylcholinesterase, TcAChE). From the paper reporting this structure, we can see the electron density around C28 is missing in the initial difference Fourier map²¹ (contoured at 4.5 sigma; see ref 21, Figure 6). Therefore, we reinterpreted the $2F_0 - F_c$ map wrapping the ligand at the 1.5 sigma level, but the electron density surrounding C28 was still absent (Figure 2A), which indicated the significant uncertainty in the predicted coordinates for C28 atom. By minimizing the PDB conformation, we found that the C28–O27–C2–C1 dihedral angle ψ rotated to 75.1° from 5.3° and this slightly altered donepezil bound conformation is shown in Figure 2B. This conformation was used as the initial ligand geometry for QM/MM X-ray refinement. The same starting geometry was also rerefined by conventional force field methods including CNS 1.3³⁸ and Refmac 5.5³⁹ (see the Methods section for details), as well as fitted into the $2F_0 - F_c$ electron density map using AFITT.^{33,40} Moreover, the donepezil geometry determined by

X-ray powder diffraction was extracted from the Cambridge Structural Database (CSD) in order to compare with modeling results based on the donepezil-TcAChE X-ray crystallography data.

Figure 3 shows the donepezil PDB deposited conformation, three rerefined X-ray structures (QM/MM, CNS, and Refmac),

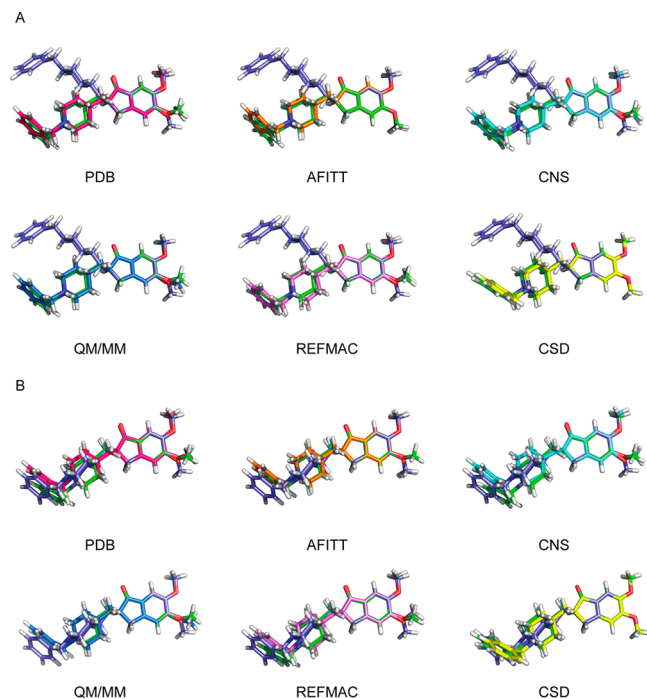


Figure 3. Superimposition of donepezil X-ray structures (PDB + CSD) plus remodeled bound conformations with their nearest local minima (green) and global minima (purple) on the potential energy surface identified by HF/6-31G* in (A) gas phase and (B) PCM solvent model.

the AFITT fitting solution and the CSD crystal structure overlapping the optimized geometries. From this figure, we can see that the position of N14 is the most obvious coordinate error existing in the original PDB conformation when compared with its fully relaxed geometries (in the gas phase and with the PCM model). This charged nitrogen in the

piperidine ring should adopt a sp^3 -hybridized configuration where the three C–N–C bond angles should be nearly identical. However, in the PDB geometry the angles are θ_1 (C_{13} – N_{14} – C_{15}) = 113.4° , θ_2 (C_{15} – N_{14} – C_{17}) = 100.9° and θ_3 (C_{17} – N_{14} – C_{13}) = 122.5° , respectively (see Table 1). This coordinate error was resolved using the QM/MM approach where θ_1 (C_{13} – N_{14} – C_{15}) = 111.3° , θ_2 (C_{15} – N_{14} – C_{17}) = 111.4° and θ_3 (C_{17} – N_{14} – C_{13}) = 112.5° (Figure 3 and Table 1). Note that AFITT also gave a good result in terms of the N14 atom position using the MMFF94 force field in its fitting process.

Another important conformational determinant of donepezil is the placement of carbon atom C8 (the only chiral center), since it controls the orientation of the piperidine and benzyl moieties within the binding pocket. The position of this asymmetric carbon atom lies above or below the C_7 – C_5 – C_4 – C_9 plane that defines the cyclopentanone envelope conformation. Here, we use the dihedral angles Φ_1 (C_4 – C_9 – C_7 – C_8) and Φ_2 (C_5 – C_7 – C_9 – C_8) that quantifies the degree to which the envelope-like conformation of the cyclopentanone ring is adopted. Their values are summarized in Table 1. From this table, we observe that the C8 atom in the donepezil PDB conformer is essentially planar (about 0.1° from planarity; see Table 1 and Figure 3) with the remaining four atoms in the cyclopentanone five-membered ring. A similar trend was observed for the CNS, Refmac, and AFITT methods with Refmac showing the most puckering. The QM/MM refinement approach puckered the cyclopentanone ring more than the other methods and the details of its impact on donepezil-TcAChE binding patterns are discussed below.

Figure 4 shows views of the modeled donepezil conformations plus the CSD geometry binding in the TcAChE active-site gorge with the amino acid residues involved in ligand recognition and stabilization highlighted (Trp84, Trp279, and Phe330). Since the quaternary ammonium, benzyl and indanone are the three major functional groups mediating donepezil-TcAChE association via π – π and cation– π interactions, the bound conformations of donepezil were further evaluated by the following metrics: (i) distance between the center of mass of the donepezil phenyl group and that of the six-membered benzene ring in the Trp84 indole functional group (d1); (ii) distance between the center of mass of the six-membered benzene ring in the donepezil 1-indanone group and

Table 1. Important Backbone Torsion Angles and Bond Angles (In Degrees) of Six Donepezil Conformations^a

gas phase						
	PDB	AFITT	CNS	QM/MM	REFMAC	CSD
Φ_1 (C_4 – C_9 – C_7 – C_8)	0.1 (10.5)	0.4 (8.9)	0.4 (7.2)	0.7 (10.5)	0.7 (10.5)	2.4 (11.2)
Φ_2 (C_5 – C_7 – C_9 – C_8)	0.7 (10.0)	0.7 (8.4)	0.6 (6.5)	1.5 (10.0)	0.6 (10.0)	2.7 (10.6)
θ_1 (C_{13} – N_{14} – C_{15})	113.4 (111.1)	111.9 (111.1)	114.4 (108.5)	111.3 (111.1)	125.7 (111.1)	110.6 (110.9)
θ_2 (C_{15} – N_{14} – C_{17})	100.9 (111.8)	110.5 (111.8)	100.7 (112.1)	111.4 (111.8)	112.8 (111.8)	112.7 (113.0)
θ_3 (C_{17} – N_{14} – C_{13})	122.5 (113.0)	112.7 (113.0)	119.5 (113.9)	112.5 (113.0)	121.5 (113.0)	109.5 (111.9)
PCM solvent model						
	PDB	AFITT	CNS	QM/MM	REFMAC	CSD
Φ_1 (C_4 – C_9 – C_7 – C_8)	0.1 (10.6)	0.4 (10.1)	0.4 (10.8)	0.7 (10.0)	0.7 (10.6)	2.4 (10.5)
Φ_2 (C_5 – C_7 – C_9 – C_8)	0.7 (9.9)	0.7 (9.4)	0.6 (10.1)	1.5 (9.8)	0.6 (9.9)	2.7 (10.6)
θ_1 (C_{13} – N_{14} – C_{15})	113.4 (111.2)	111.9 (111.2)	114.4 (111.2)	111.3 (111.1)	125.7 (111.2)	110.6 (110.9)
θ_2 (C_{15} – N_{14} – C_{17})	100.9 (111.0)	110.5 (111.0)	100.7 (111.0)	111.4 (111.8)	112.8 (111.0)	112.7 (113.0)
θ_3 (C_{17} – N_{14} – C_{13})	122.5 (113.1)	112.7 (113.1)	119.5 (113.0)	112.5 (113.0)	121.5 (113.1)	109.5 (111.9)

^aThe figures in parentheses are the corresponding angle values of their optimized geometries identified by HF/6-31G* in gas phase and PCM solvent model.

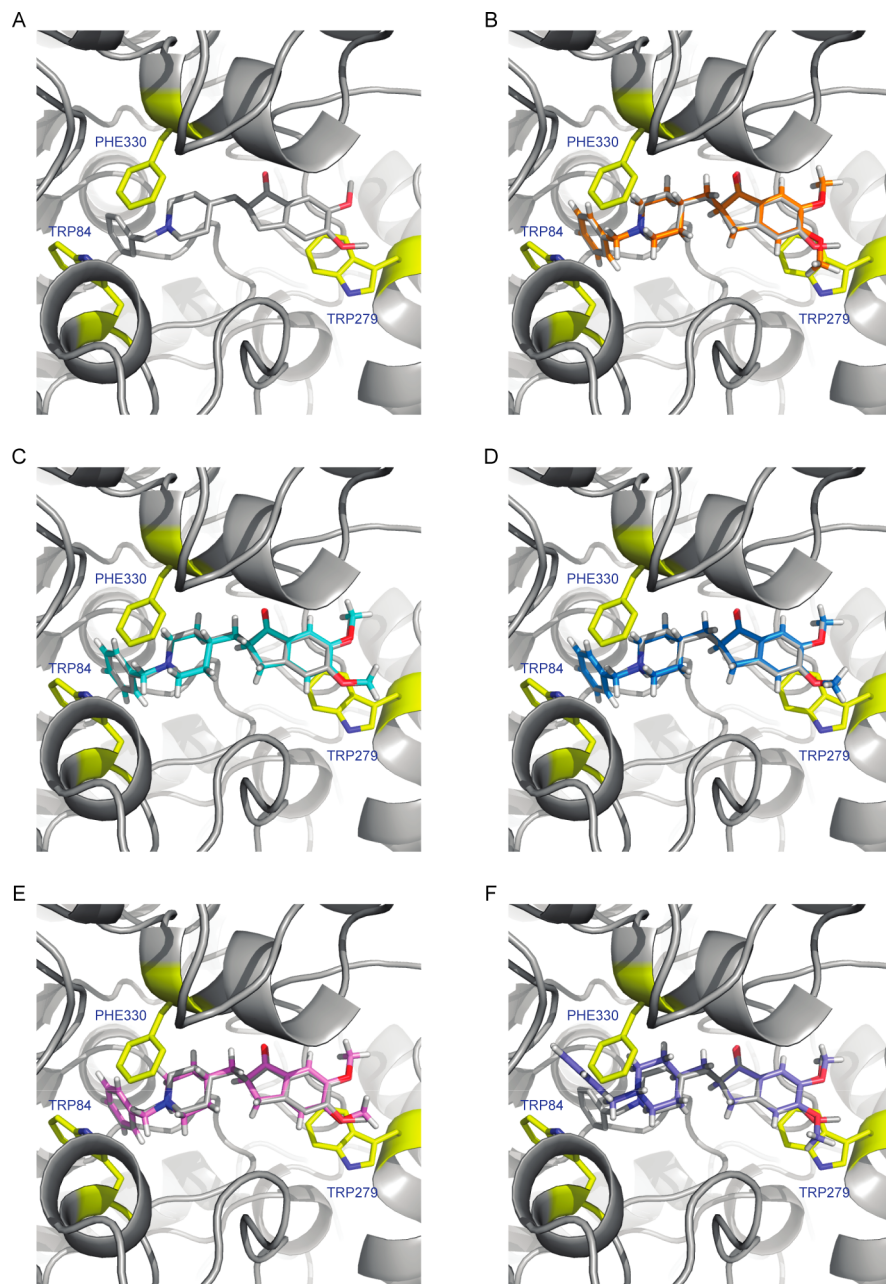


Figure 4. (A) Original donepezil bound conformation in the context of the active site gorge of TcAChE; overlays of PDB deposited donepezil conformer (white) and (B) AFITT fitting result (orange); (C) CNS rerefined structure (cyan); (D) parallel QM/MM rerefined structure (blue); (E) Refmac5 rerefined structure (pink); (F) crystal structure extracted from Cambridge Structural Database (yellow).

that of the aromatic ring of Trp279 (d2) and (iii) the distance between N14 and the center of mass of the Phe330 benzyl ring (d3). Table 2 and Supporting Information Figure 2 lists these three distances for the various donepezil-TcAChE modeled structures.

For the distance between the donepezil phenyl group and the aromatic ring of Trp84, the QM/MM refinement yields d1 = 3.86 Å that is in good agreement with the theoretical studies of $\pi-\pi$ interaction on the benzene dimer by Sinnokrot and co-workers.⁴¹ They reported that the separation in the benzene dimer was 3.7 Å in the sandwich configuration using MP2/aug-cc-pVTZ optimized geometries. This arises because the QM/MM refinement reduced the deviation from an ideal envelope conformation for the C4–C5–C7–C8–C9 torsion of the cyclopentanone ring, which in turn altered the spatial

Table 2. Strain Energies (in kcal/mol) of AFITT Fitting Result, CSD Crystal Structure, PDB Deposited Donepezil Conformer, and Its Re-refined Geometries in Vacuo and in PCM Solvent Model

		PDB	AFITT	CNS	QM/MM	REFMAC	CSD
gas	local	55.3	17.0	74.1	4.4	75.6	252.8
	global	63.3	22.5	79.0	12.4	83.6	260.8
PCM	local	55.2	16.0	71.0	3.8	72.3	252.7
	global	60.3	17.7	76.1	9.7	77.4	254.7

orientation of the donepezil benzyl group. From Figure 3, we can find that comparing with the other modeling approaches, the phenyl group of the QM/MM refined donepezil conformer

Table 3. Distances (\AA) of Cation– π and π – π Interaction Involved in Donepezil-TcAChE Recognition and Association

	PDB	AFITT	CNS	QM/MM	REFMAC
d1 (Trp84 --- benzyl group)	3.88	3.92	3.88	3.86	3.87
d2 (Trp279 --- 1-indanone group)	4.07	4.10	4.07	4.11	4.17
d3 (Phe330 -- N ⁺)	4.06	4.10	4.08	4.12	3.93

overlaps the counterpart of its fully relaxed geometry (in vacuo and in solution) to the maximum extent. Nonetheless, for this interaction all methods do a reasonable job of modeling the d1 distance. Sinnokrot et al. also found that the parallel benzene dimer plane was separated by 3.8 \AA in the parallel-displaced configuration yet all modeling results have the d2 value at least 0.27 \AA higher than this value. One possible explanation is the fact that the benzene dimer is not the optimal reference system for comparison with the π – π interaction between the six-membered ring within indole due to electronic differences between indole and benzene.

For the d3 value, we use Felder and co-workers study⁴² on cation– π interactions between tetramethylammonium and benzene as a reference to evaluate the different modeling methods. They reported that the distance between the charged nitrogen atom of tetramethylammonium and the center of benzene was 4.18 \AA estimated by the MP2/6-31G* level of theory (configuration 1, see ref 41). Our QM/MM and AFITT results agree well with their computational outcome since only these two methods corrected the N14 atom coordinate position. The d3 value for Refmac was 0.25 \AA lower than the MP2/6-31G* result mainly due to the sp^2 -hybridized configuration of the N14 atom in its rerefined structure (see Table 1 and Supporting Information Figure 2).

Strain Energy. One useful tool for evaluating the quality of modeled donepezil conformations is their strain energies. Conformational features far from being “ideal” will lead to a distorted structure with high strain energy. In this study, the strain energy was defined as the single-point energy difference between a conformer and its fully optimized geometry (thought to be “strain free”). MP2/CBS single-point energy calculations were employed to calculate the strain energy for the five donepezil bound conformations plus the CSD geometry with respect to the nearest local minimum (local strain) and global minimum (global strain) on the donepezil conformational energy surface (see Figure 3 for local/global minimum conformations). As shown in Table 3, the QM/MM refinement method generated the lowest local strain energy when compared with other modeling methods (4.4 kcal/mol in gas phase and 3.8 kcal/mol in PCM solvent model). The AFITT fitting protocol successfully corrected the configuration of the quaternary ammonium yet it retained the planar conformation of the five-membered cyclopentanone ring yielding a 17.0 kcal/mol local strain energy in the gas phase and 16.0 kcal/mol in the continuum solvent model. Three conventional force field modeling approaches (PDB, CNS, and Refmac) neither corrected the position of the charged nitrogen atom nor appropriately placed the chiral carbon atom in the 1-indanone group. Therefore, their local strain energies ranged from 55.3 kcal/mol to 75.6 kcal/mol in vacuo and from 55.2 kcal/mol to 72.3 kcal/mol in solvent, with average values of 68.3 and 66.2 kcal/mol, respectively. The extremely high local strain energy of the CSD conformation originates from the rotation of the N14–C17 single bond that in turn gives rise to an energetically unfavorable conformation. From Figure 3, we can clearly observe that the phenyl group of CSD donepezil conformation

nearly touches the Phe330 residue located in the TcAChE active site.

It is worthwhile to point out that the global strain of the QM/MM rerefined conformer was about 8 kcal/mol higher than its local strain in the gas phase and 6 kcal/mol higher in aqueous solution, respectively. We ascribe these energy differences to the rotation of the C8–C10 and C10–C11 sigma bonds in the global minimum conformations (gas phase and solvent) that in turn altered the orientation of the piperidine and benzyl rings relative to the rerefined geometry and induced more conformational strain (Figure 3). However, given the narrow shape of TcAChE active-site gorge, these low energy conformations do not fit well into the binding pockets and so are likely not to be the “bioactive” conformations (Figure 3 and 4). Another possible factor contributing to this phenomenon was the location of the C28 atom (Figure 3). Recall that we used ψ (C28–O27–C2–C1) = 75.1° to place the C28 atom in the initial structure of donepezil for modeling (Figure 2) and after QM/MM refinement the dihedral angle ψ (C28–O27–C2–C1) was 96.4°. Whereas the most energy favorable conformations identified by Omega plus HF/6-31G* (gas phase and solvent) both have ψ (C28–O27–C2–C1) = 180°, which were in agreement with the CSD geometry and the AFITT modeling result. Note that CNS and Refmac both returned this dihedral angle back to about 5° just as observed in the original PDB conformation.

CONCLUSIONS

In the present study, we first carried out single point calculations on 18 free state donepezil low-energy conformations using MP2/CBS and M06 functionals, which enabled a detailed and accurate understanding of the donepezil conformational energy surface. Further molecular modeling and conformational analysis for bound donepezil conformations were performed with using QM/MM X-ray refinement, CNS, Refmac, and AFITT fitting. Ab initio geometry optimizations at the HF/6-31G* level of theory were executed on each of these modeled conformers along with the CSD geometry. Compared with the fully relaxed geometry in the gas phase as well as in a continuum solvent model, the original PDB structure incorrectly positioned the charged N14 atom that plays a key role in cation– π interactions with the Phe330 benzyl ring. Moreover, another notable difference between the PDB deposited conformation and its optimized geometry was the extreme flattening of the envelope conformation of the cyclopentanone ring as a result of misplacing the chiral center located on the indanone functional group along with force field errors in modeling five-membered rings. Our QM/MM refinement approach improved these two coordinate errors and consequently adjusted the quaternary ammonium–Phe330 donepezil and phenyl group–Trp84 distances, which yielded good agreement with results from previous theoretical studies using highly accurate levels of theory. Moreover, QM/MM refinement largely released the conformational strain existing in the PDB deposited structure and reduced the local strain energy to 3.8 kcal/mol in aqueous solution and 4.4 kcal/mol in

vacuo. Other modeling methodologies did improve some aspects of the structure but largely retained significant strain energies of greater than 17 kcal/mol.

MATERIAL AND METHODS

Exploring Donepezil Conformational Energy Surface.

Omega version 2.4.3³³ from Openeye Scientific Software was employed to generate a conformational ensemble for donepezil. Jonas Boström et al. evaluated the performance of Omega with different parameter settings in 2003,⁴³ and according to their analysis, we selected a 5 kcal/mol cutoff (“-ewindow 5”) with the MMFF94s force field. Parameters “-maxconf” and “-rms” were both set to zero that ensure Omega output all unique donepezil conformations. Since our QM/MM X-ray refinement protocol used the HF/6-31G* level of theory as the Hamiltonian to optimize the donepezil bound conformations, further gas-phase geometry optimizations employed the same model chemistry. The Gaussian 09 suite of programs⁴⁴ were chosen to perform all ab initio geometry optimizations with the keyword “Opt = VeryTight”, to fully relax all local and global minimum conformations.

Single-Point Energy Calculation. To describe the details of the donepezil conformational energy surface, we performed single-point calculations, in the gas phase, for all Omega/ab initio QM identified low-energy conformers at several different level of theories computed with Gaussian 09 (including M06L/6-311+G**, M06L/aug-cc-pVDZ, M06-2x/6-311+G**, M06-2x/aug-cc-pVDZ, M06-2x/aug-cc-pVTZ, M06/6-311+G**, M06/aug-cc-pVDZ, and M06/aug-cc-pVTZ). We employed MP2 complete basis set (CBS) calculations as benchmarks and compared the MP2/CBS outcomes with several DFT methods. For a more mathematical description about the strategy of CBS extrapolation, please refer to our previous work on ibuprofen and retinoic acid.^{35,36}

Parallel QM/MM X-ray Crystallography Refinement. In ab initio molecular orbital calculations, the most time-consuming step is computing the so-called electron repulsion integrals (ERI),

$$\text{ERI} = \iint \psi_\mu(r_1)\psi_\nu(r_1) \frac{1}{r_{12}} \psi_\lambda(r_2)\psi_\sigma(r_2) \, dr_1 \, dr_2$$

Calculating these two-electron integrals typically uses the direct self-consistent field (SCF) approach to generate the Fock matrix. The Fock matrix is defined as

$$F_{\mu\nu} = H_{\mu\nu}^{\text{core}} + \sum_{\lambda} \sum_{\sigma} P_{\lambda\sigma} \left[(\mu\nu|\lambda\sigma) - \frac{1}{2} (\mu\lambda|\nu\sigma) \right]$$

where $H_{\mu\nu}^{\text{core}}$ is the one-electron integral matrix for the fixed nuclei, $P_{\lambda\sigma}$ is the density matrix, $(\mu\nu|\lambda\sigma)$ represents the two-electron coulomb integrals, and $(\mu\lambda|\nu\sigma)$ represent the two-electron exchange integrals. Herein, we implemented distributed data parallel algorithms⁴⁵ into our in-house package QUICK with the MPI (Message Passing Interface) library so as to increase the computational efficiency of the two-electron Coulomb and exchange integrals in the Fock matrix assembly step. Further details are given in the Supporting Information section.

ASSOCIATED CONTENT

Supporting Information

3D structures of 18 donepezil low-energy conformers. R code and output of nonparametric statistical inferences on

comparing MP2/CBS and DFT methods. Parameter setting of CNS and Refmac refinement procedure. Pseudocode of parallel algorithm for computing 2-electron ERI in QM/MM refinement. This material is available free of charge via the Internet at <http://pubs.acs.org>.

AUTHOR INFORMATION

Corresponding Author

*Phone: 352-392-6973. Fax: 352-392-8722. E-mail: merz@qtp.ufl.edu.

Notes

The authors declare no competing financial interest.

ACKNOWLEDGMENTS

We thank the National Institutes of Health (SBIR GM079899 and RO1's GM044974 and GM066859) for financial support of this research. Computing support from the University of Florida High Performance Computing Center is gratefully acknowledged.

REFERENCES

- (1) Cummings, J. L.; Back, C. *Am. J. Geriatr. Psychiatry* **1998**, *6*, S64.
- (2) Bartus, R. T.; Dean, R. L., 3rd; Beer, B.; Lippa, A. S. *Science* **1982**, *217*, 408.
- (3) Babic, T. *J. Neurol. Neurosurg. Psychiatry* **1999**, *67*, 558.
- (4) Davidsson, P.; Blennow, K.; Andreasen, N.; Eriksson, B.; Minthon, L.; Hesse, C. *Neurosci. Lett.* **2001**, *300*, 157.
- (5) Sugimoto, H.; Ogura, H.; Arai, Y.; Iimura, Y.; Yamanishi, Y. *Jpn. J. Pharmacol.* **2002**, *89*, 7.
- (6) Liston, D. R.; Nielsen, J. A.; Villalobos, A.; Chapin, D.; Jones, S. B.; Hubbard, S. T.; Shalaby, I. A.; Ramirez, A.; Nason, D.; White, W. F. *Eur. J. Pharmacol.* **2004**, *486*, 9.
- (7) Mohs, R. C.; Doody, R. S.; Morris, J. C.; Ieni, J. R.; Rogers, S. L.; Perdomo, C. A.; Pratt, R. D.; Grp, S. *Neurol.* **2001**, *57*, 481.
- (8) Trinh, N. H.; Hoblyn, J.; Mohanty, S. U.; Yaffe, K. *J. Am. Med. Assoc.* **2003**, *289*, 210.
- (9) Gauthier, S.; Feldman, H.; Hecker, J.; Vellas, B.; Subbiah, P.; Whalen, E. *J. Am. Geriatr. Soc.* **2000**, *48*, S2.
- (10) Gauthier, S.; Feldman, H.; Hecker, J.; Vellas, B.; Ames, D.; Subbiah, P.; Whalen, E.; Emir, B.; Investigators, D. M. S. *Int. Psychogeriatr.* **2002**, *14*, 389.
- (11) Holmes, C.; Wilkinson, D.; Dean, C.; Vethanayagam, S.; Olivieri, S.; Langley, A.; Pandita-Gunawardena, N. D.; Hogg, F.; Clare, C.; Damms, J. *Neurol.* **2004**, *63*, 214.
- (12) Kaufer, D. I.; Catt, K.; Pollock, B. G.; Lopez, O. M.; DeKosky, S. T. *Neurol.* **1998**, *50*, A89.
- (13) Harry, R. D. J.; Zekyanis, K. K. *Hum. Psychopharm. Clin.* **2005**, *20*, 183.
- (14) Wilcock, G.; Howe, I.; Coles, H.; Lilienfeld, S.; Trynen, L.; Zhu, Y.; Bullock, R.; Grp, G. G. S. *Drug Aging* **2003**, *20*, 777.
- (15) Rogers, S. L.; Doody, R. S.; Mohs, R. C.; Friedhoff, L. T.; Grp, D. S. *Arch. Intern. Med.* **1998**, *158*, 1021.
- (16) Winblad, B.; Kilander, L.; Eriksson, S.; Minthon, L.; Batsman, S.; Wetterholm, A. L.; Jansson-Blixt, C.; Haglund, A. *Lancet* **2006**, *367*, 1057.
- (17) Sugimoto, H.; Tsuchiya, Y.; Sugumi, H.; Higurashi, K.; Karibe, N.; Iimura, Y.; Sasaki, A.; Araki, S.; Yamanishi, Y.; Yamatsu, K. *J. Med. Chem.* **1992**, *35*, 4542.
- (18) Sugimoto, H.; Iimura, Y.; Yamanishi, Y.; Yamatsu, K. *J. Med. Chem.* **1995**, *38*, 4821.
- (19) Sussman, J. L.; Harel, M.; Frolow, F.; Oefner, C.; Goldman, A.; Toker, L.; Silman, I. *Science* **1991**, *253*, 872.
- (20) Kryger, G.; Silman, I.; Sussman, J. L. *J. Physiol. Paris* **1998**, *92*, 191.
- (21) Kryger, G.; Silman, I.; Sussman, J. L. *Structure* **1999**, *7*, 297.

- (22) Doucet-Personeni, C.; Bentley, P. D.; Fletcher, R. J.; Kinkaid, A.; Kryger, G.; Pirard, B.; Taylor, A.; Taylor, R.; Taylor, J.; Viner, R.; Silman, I.; Sussman, J. L.; Greenblatt, H. M.; Lewis, T. *J. Med. Chem.* **2001**, *44*, 3203.
- (23) da Silva, C. H.; Campo, V. L.; Carvalho, I.; Taft, C. A. *J. Mol. Graphics Modell.* **2006**, *25*, 169.
- (24) Remya, C.; Dileep, K. V.; Tintu, I.; Variyar, E. J.; Sadasivan, C. *Med. Chem. Res.* **2012**, *21*, 2779.
- (25) Deb, P. K.; Sharma, A.; Piplani, P.; Akkinapally, R. R. *Mol. Divers.* **2012**, in press.
- (26) Niu, C.; Xu, Y.; Luo, X.; Duan, W.; Silman, I.; Sussman, J. L.; Zhu, W.; Chen, K.; Shen, J.; Jiang, H. *J. Phys. Chem. B* **2005**, *109*, 23730.
- (27) Guo, J.; Hurley, M. M.; Wright, J. B.; Lushington, G. H. *J. Med. Chem.* **2004**, *47*, 5492.
- (28) Yu, N.; Yennawar, H. P.; Merz, K. M., Jr. *Acta Crystallogr. D Biol. Crystallogr.* **2005**, *61*, 322.
- (29) Yu, N.; Li, X.; Cui, G.; Hayik, S. A.; Merz, K. M., 2nd *Protein Sci.* **2006**, *15*, 2773.
- (30) Yu, N.; Hayik, S. A.; Wang, B.; Liao, N.; Reynolds, C. H.; Merz, K. M. *J. Chem. Theory Comput.* **2006**, *2*, 1057.
- (31) Li, X.; He, X.; Wang, B.; Merz, K., Jr. *J. Am. Chem. Soc.* **2009**, *131*, 7742.
- (32) Li, X.; Hayik, S. A.; Merz, K. M., Jr. *J. Inorg. Biochem.* **2010**, *104*, 512.
- (33) *OEChem*, version 1.7.4, OpenEye Scientific Software, Inc., Santa Fe, NM, USA, www.eyesopen.com, 2010.
- (34) Merz, K. M.; Molnar, L. F.; He, X.; Wang, B. *J. Chem. Phys.* **2009**, *131*.
- (35) Fu, Z.; Li, X.; Merz, K. M., Jr. *J. Comput. Chem.* **2011**, *32*, 2587.
- (36) Fu, Z.; Li, X.; Merz, K. M., Jr. *J. Chem. Theory Comput.* **2012**, *8*, 1436.
- (37) Li, X.; Fu, Z.; Merz, K. M., Jr. *J. Comput. Chem.* **2012**, *33*, 301.
- (38) Brunger, A. T.; Adams, P. D.; Clore, G. M.; DeLano, W. L.; Gros, P.; Grosse-Kunstleve, R. W.; Jiang, J. S.; Kuszewski, J.; Nilges, M.; Pannu, N. S.; Read, R. J.; Rice, L. M.; Simonson, T.; Warren, G. L. *Acta Crystallogr. D* **1998**, *54*, 905.
- (39) Vagin, A. A.; Steiner, R. A.; Lebedev, A. A.; Potterton, L.; McNicholas, S.; Long, F.; Murshudov, G. N. *Acta Crystallogr. D* **2004**, *60*, 2184.
- (40) Wlodek, S.; Skillman, A. G.; Nicholls, A. *Acta Crystallogr. D Biol. Crystallogr.* **2006**, *62*, 741.
- (41) Sinnokrot, M. O.; Valeev, E. F.; Sherrill, C. D. *J. Am. Chem. Soc.* **2002**, *124*, 10887.
- (42) Felder, C.; Jiang, H. L.; Zhu, W. L.; Chen, K. X.; Silman, I.; Botti, S. A.; Sussman, J. L. *J. Phys. Chem. A* **2001**, *105*, 1326.
- (43) Bostrom, J.; Greenwood, J. R.; Gottfries, J. *J. Mol. Graphics Modell.* **2003**, *21*, 449.
- (44) Frisch, M. J.; Trucks, G. W.; Schlegel, H. B.; Scuseria, G. E.; Robb, M. A.; Cheeseman, J. R.; Scalmani, G.; Barone, V.; Mennucci, B.; Petersson, G. A.; Nakatsuji, H.; Caricato, M.; Li, X.; Hratchian, H. P.; Izmaylov, A. F.; Bloino, J.; Zheng, G.; Sonnenberg, J. L.; Hada, M.; Ehara, M.; Toyota, K.; Fukuda, R.; Hasegawa, J.; Ishida, M.; Nakajima, T.; Honda, Y.; Kitao, O.; Nakai, H.; Vreven, T.; Montgomery, J. A., Jr.; Peralta, J. E.; Ogliaro, F.; Bearpark, M.; Heyd, J. J.; Brothers, E.; Kudin, K. N.; Staroverov, V. N.; Kobayashi, R.; Normand, J.; Raghavachari, K.; Rendell, A.; Burant, J. C.; Iyengar, S. S.; Tomasi, J.; Cossi, M.; Rega, N.; Millam, N. J.; Klene, M.; Knox, J. E.; Cross, J. B.; Bakken, V.; Adamo, C.; Jaramillo, J.; Gomperts, R.; Stratmann, R. E.; Yazyev, O.; Austin, A. J.; Cammi, R.; Pomelli, C.; Ochterski, J. W.; Martin, R. L.; Morokuma, K.; Zakrzewski, V. G.; Voth, G. A.; Salvador, P.; Dannenberg, J. J.; Dapprich, S.; Daniels, A. D.; Farkas, Ö.; Foresman, J. B.; Ortiz, J. V.; Cioslowski, J.; Fox, D. J. *Gaussian 09*, Revision A.1; Gaussian, Inc.: Wallingford, CT, 2009.
- (45) Alexeev, Y.; Kendall, R. A.; Gordon, M. S. *Comput. Phys. Commun.* **2002**, *143*, 69.